PRECLINICAL RESEARCH

Mitral Butterfly

Preclinical Experience of a Novel Chordal Repair Device Using an Artificial Papillary Muscle

Johanna M. Ticar, MMSc,[a],* Gediminas Gaidulis, PhD,[b],* Kenzie Veith, MSc,[c],* Claus Rath, MD,[d] Jeremy Jarman, BSc,[a] Werner Mohl, MD, PhD[a,e]

VISUAL ABSTRACT

healthy mitral valve — chordae prevent excessive systolic motion

diseased — damaged chordae resulting in regurgitation

conventional repair — multiple individual chords placed-attachment to myocardium

mitral butterfly — single implant placed encompassing entire leaflet segment-myocardium spared

90-day study

7 healthy pigs with normal EOA and PMG

Device implanted via trans-atrial delivery onto the posterior leaflet

Serial echo and angiography used at 30, 60, 90 days post op

atrial | ventricular

Mitral butterfly: provides support for flailing leaflet-
NO chordal adjustment
NO anchorage in myocardium

Trial outcomes
- Successful implantation
- Deployment time < 2 minutes
- NO regurgitation or stenosis
- Stable device integration
- NO extraneous tissue damage

FEA analysis: simulated implantation
↑ coaptation ↓ chordal stress

Echo evaluation: NO MR or MS

Ticar, J.M. et al. J Am Coll Cardiol Basic Trans Science. 2020;5(10):1002–14.

HIGHLIGHTS

- **MR continues to be a challenge encountered in clinical practice. If left untreated, the effects are far reaching with LV volume overload, pulmonary hypertension, and potentially progression into severe heart failure. Many patients are not routinely offered surgery because of comorbidities and perceived surgical risk.**

- **The Mitral Butterfly is a novel device offering minimally invasive repair of a prolapsing valve with a simple, single-step deployment. This catheter-based device is composed of a nitinol frame and a polymer matrix covering the entire prolapsing segment of the insufficient valve. Unlike other chordal repair techniques, there is no need for myocardial fixation.**

- **Device performance in a 90-day chronic animal study and in silico analysis substantiated the underlying device concept.**

- **Progress continues to be made in developing a safe and effective transcatheter alternative for MV repair.**

SUMMARY

Transcatheter mitral repair is based on the principle of artificial monochordal repair. In this paper, the authors show an alternative, based on the realization of an artificial papillary muscle concept that avoids multiple chordal replacements and fixation in the myocardium. Unlike the interposition of artificial chordae between the free edge of the leaflet and the myocardium, the so-called Mitral Butterfly device collects a multitude of chordae in a matrix connected to a swing arm, stabilizing prolapsing forces with a broad atrial support. Device testing in chronic animal models and in silico substantiated the underlying device concept and performance after 90 days. (J Am Coll Cardiol Basic Trans Science 2020;5:1002–14) © 2020 The Authors. Published by Elsevier on behalf of the American College of Cardiology Foundation. This is an open access article under the CC BY-NC-ND license (http://creativecommons.org/licenses/by-nc-nd/4.0/).

**ABBREVIATIONS
AND ACRONYMS**

LA = left atrium (atrial)

LV = left ventricle (ventricular)

MR = mitral regurgitation

MV = mitral valve

PET = polyethylene terephthalate

PM = papillary muscle

Since the introduction of the Carpentier technique in 1966, surgical mitral valve (MV) repair has been the standard corrective treatment for degenerative mitral regurgitation (MR). Typically characterized by MV prolapse (1), degenerative MR is mitral insufficiency as a result of damage to structural elements of the mitral apparatus, as opposed to functional MR, in which global ventricular changes eventually affect the geometry of the valve. Whereas degenerative MR has a localized beginning, if left untreated the effects are far reaching with left ventricular (LV) volume overload leading to annular dilatation and further valve insufficiency, followed by atrial fibrillation, pulmonary hypertension, and subsequent progression into severe heart failure and death. Open heart procedures in general are invasive and carry a high surgical risk, many (especially elderly) patients are therefore not routinely offered corrective surgery (2,3).

Transcatheter MV repair solutions are being explored globally, having a less invasive approach and expectedly fewer contraindications, these techniques are already showing potential in addressing the unmet clinical needs. Furthermore, many catheter-based systems are designed to approximate their surgical alternatives, in this way adhering to established standards while reducing the surgical burden and widening the patient pool. One such technique is minimally invasive chordal repair, where sequential insertion of artificial chordae to replace broken or elongated chordae has shown promising results and typically the MV leaflets are spared and valve function is restored by altering the tension of newly implanted chordae. In the last decade, this repair technique has been performed via a right minithoracotomy on extracorporeal circulation and cardiac arrest or off-pump by entering the LV via apical access, and the first transseptal options are currently being developed. To allow proper force distribution on prolapsing segments, a multitude of artificial chordae (n ≥ 2) are deployed, subsequently tensioned under echo guidance and secured at the myocardium (4). The orientation of artificial chordae and their attachment to muscular structures is critical in terms of biomechanical behavior as nonphysiological stress acting on the native tissue may result in suboptimal MV repair (5,6).

The Mitral Butterfly (AVVie, Vienna, Austria) is a novel transcatheter device, which can be either surgically placed via the left atrium (LA) or by a completely percutaneous (transfemoral-transseptal) approach. The transseptal approach for the Mitral Butterfly is currently under development but has not yet undergone chronic testing. The device is based on the concept of an artificial papillary muscle (PM), where a ventricular element provides a fixation point for a multitude of chordae that, along with a polymer mesh, contain the entire prolapsing segment. The implant is stabilized via a transleaflet clasp near the annulus and makes use of atrial support designed to counteract the closing forces and prevent excessive leaflet motion.

In this paper, for the first time, we report on device performance analyzed from a virtual implantation (computational analysis) of the Mitral Butterfly device as well as serial functional assessments in a chronic animal study.

FIGURE 1   Components of the Mitral Butterfly Device
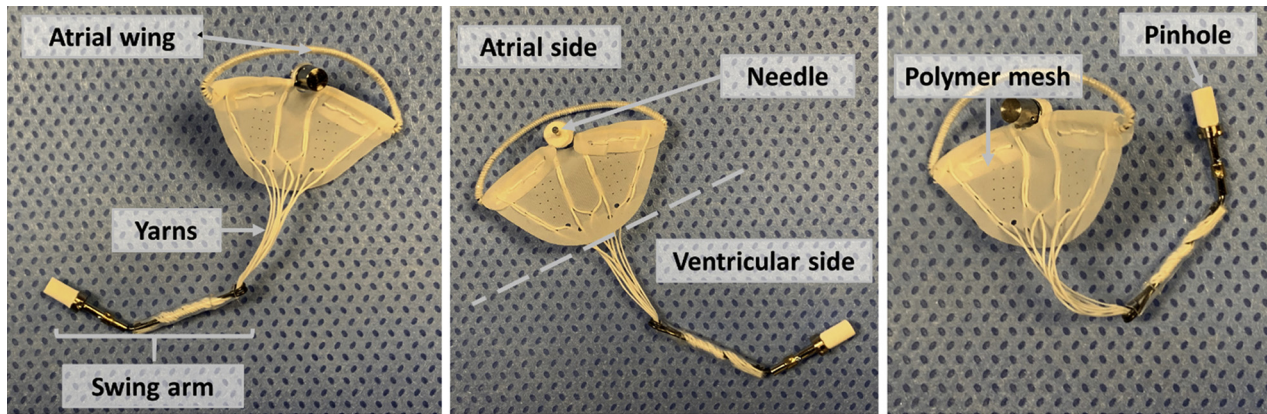
These panels show the individual components of the device (atrial wing, needle and polymer mesh on the atrial side; pinhole, swing arm and yarns on the ventricular side).

METHODS

TECHNICAL DESCRIPTION OF DEVICE. The Mitral Butterfly (AVVie GmbH, Vienna, Austria) is a catheter-based device consisting of a collapsible nitinol frame (atrial wing and swing arm), a polymer matrix (poly-ethylene terephthalate [PET] mesh and polytetra-fluoroethylene [PTFE] yarns), and a clasp (needle and pinhole). **Figure 1** illustrates the components of the implant.

The polymer matrix is composed of a mesh with inclusions of polytetrafluoroethylene yarns (Lenzing Plastics, Lenzing, Austria) that extends from the nitinol wing along the annulus toward a swing arm in the LV, covering the entire prolapsing segment of the insufficient valve.

The implant is designed to pivot with the motion of the native valve, allowing unrestricted flow in dias-tole, but limiting the range of leaflet motion in sys-tole. This rocking action is achieved by anchoring the

FIGURE 2   Mitral Butterfly in a Passive Perfused Heart Model
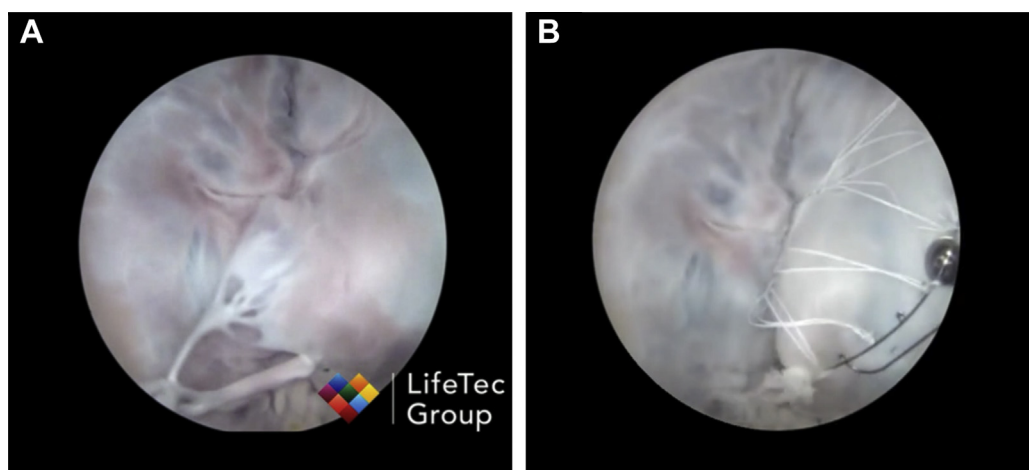
The Mitral Butterfly has been tested in a passive perfused heart model (Lifetec Group, Eindhoven, the Netherlands). **(A)** Mitral valve prolapse induced by cutting chordae. **(B)** The Mitral Butterfly implant repairs the prolapse by containing the leaflet. See Videos 1 and 2.

FIGURE 3 Mitral Butterfly Attachment Process

(A) Transcatheter deployment of the Mitral Butterfly device. **(B)** Implant attachment with a single clasp in the peri-annular region.
(C) Deployed Mitral Butterfly device restoring a normal coaptation plane.
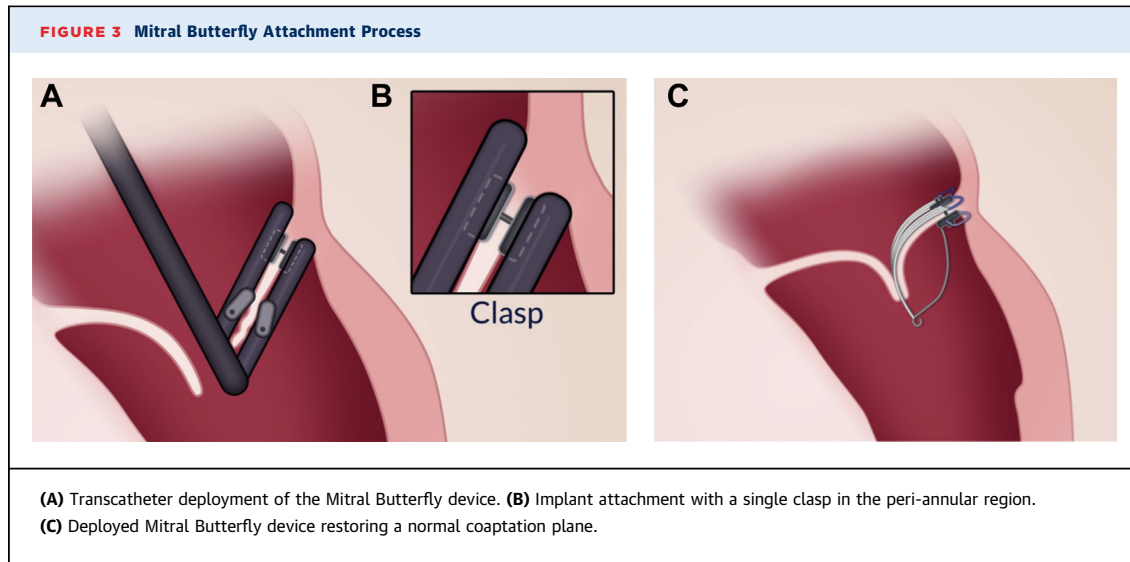
implant with a single clasp in the peri-annular region of the prolapsing valve segment, when the MV opens, the implant swings with the native leaflet and blood moves freely through the mitral orifice. As ventricular pressure rises, the native leaflets and consequently also the implant, move together toward a closed position. To prevent the implant from rocking further than desired, an atrial support element, known as the wing, contacts the atrial wall and arrests the implant. This interaction counters the ventricular forces, stabilizes the swing arm, and allows the polymer mesh and chordae to restrain the previously prolapsing segment.

This seesaw action of the implant, which has already been proven feasible in bench testing (**Figure 2** and **Videos 1 and 2**), essentially mimics the function of a PM

without the need for myocardial fixation, typically seen in chordal repair techniques. A key feature of the device is the 1-step implantation strategy: once positioned correctly, the needle of the clasp is pierced through the leaflet to engage with the locking cap on the swing arm. This simple clasping action not only fixes the implant in place but also ensures the correct deployment of the polymer mesh and a multitude of chordae, which, in contrast to other techniques, require no further tensioning (**Figure 3**). In addition to the needle, a button made of titanium is used as a backer for a compressible material to prevent local necrosis and passage through the leaflet.

Alignment to the annulus is maintained by the shape of the atrial wing, ensuring adequate structural support. The Mitral Butterfly is primarily designed for

FIGURE 4 Depiction of Delivery System

Depiction of the 24-F transatrial delivery system with 2 arms at the distal end housing the upper (atrial wing and polymer mesh) and lower (swing arm) parts of the implant. The upper (atrial) arm is placed above the leaflet, and the lower (ventricular) arm is wedged underneath the leaflet during device placement. See Video 3.
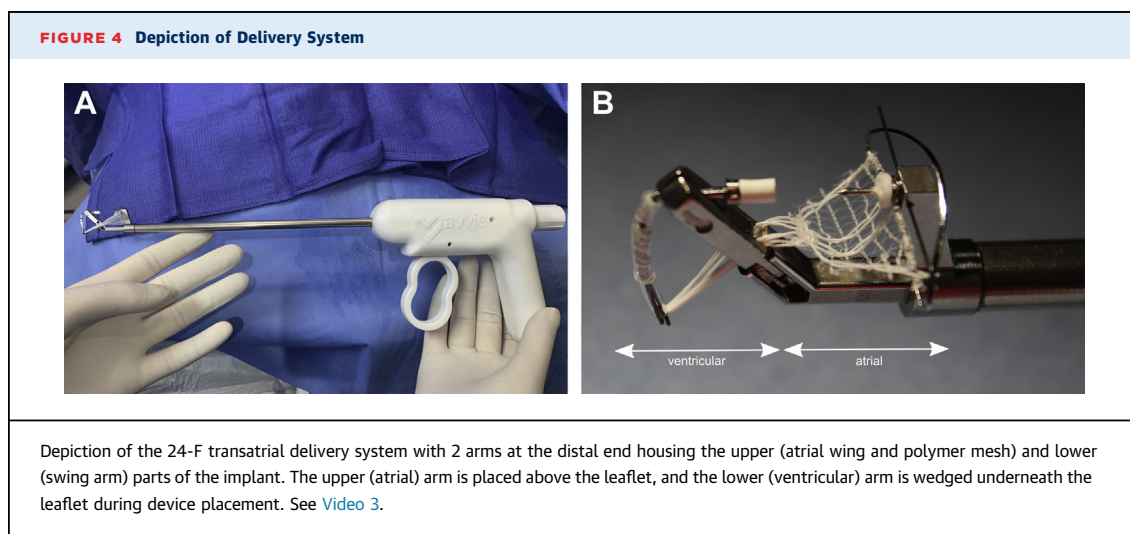
TABLE 1   Material Parameters for Mitral Butterfly Elements

Material	Element(s)	Young Modulus (MPa)	Poisson Ratio
PTFE	Neochordae	500	0.48
Nitinol	Swing arm Atrial wing	75×10^3	0.33
Titanium	Needle Button	110×10^3	0.35
Stainless steel	Locking collar	190×10^3	0.25
Felt	Upper felt fitting Lower felt fitting	34	0.35

PTFE = polytetrafluoroethylene.

use on the posterior (P2/P3) segment, which is most commonly affected by MV prolapse (7). However, it has also been successfully applied in passive perfused hearts to anterior leaflet prolapse. The wing and swing arm are connected by leaflet penetration; hence, no additional attachment to muscular structures is necessary. The implant can be either deployed via a 24-F transatrial (mini-thoracotomy) or completely percutaneous (transfemoral-transseptal) approach. The transfemoral-transseptal delivery tool is currently under development. The transatrial delivery tool (**Figure 4**) has 2 arms at the distal end housing the upper (atrial wing and polymer mesh) and lower (swing arm) parts of the implant. The upper (atrial) arm is placed above the leaflet, and the lower (ventricular) arm is wedged underneath the leaflet. When the device is at the target location, the upper and lower arms of the delivery tool are brought into apposition allowing the needle to pierce the leaflet and engage with the locking cap. Once engaged, both the swing arm and the atrial wing can then be released from the delivery tool (Video 3).

COMPUTATIONAL ANALYSIS. To better understand the mechanism of MV prolapse repair after the implantation of the Mitral Butterfly as well as to increase the validity of the presented implant (**Figure 1**), a computational study using a finite element method was performed.

For this, a structural model of the prolapsing MV described in the previous work (8) was used. Briefly, the geometry of the MV was reconstructed from transesophageal echocardiographic images, obtained using the Vivid E95 ultrasound machine (GE Healthcare, Princeton, New Jersey) at the heart rate of 66 beats/min, characterized by a 22-Hz time frequency. Image segmentation and mesh generation were performed using a custom platform developed in MATLAB (MathWorks, Natick, Massachusetts), which was described in detail by Stevanella et al. (9). Regionally varying thickness was assigned to the MV leaflets, as suggested by Kunzelman et al. (10), with

the average values of 1.32 and 1.26 mm for the anterior and posterior leaflets, respectively. The model was completed by adding the tips of anterolateral and posteromedial PMs and a branched network of marginal, basal, and strut chordae with constant cross-sectional area values of 0.40, 0.79, and 1.15 mm², respectively. The chordae tendineae were removed from the middle segment of the posterior leaflet (P2), thus allowing to stimulate MV prolapse.

The mechanical behavior of the MV leaflets was assumed to be nonlinear and anisotropic and was described through a constitutive model that was proposed by Lee et al. (11). To characterize nonlinear and isotropic mechanical behavior of the chordae tendineae, a second-order polynomial hyperelastic model was chosen. Both PM tips were treated as single nodes without any physical properties.

A time-dependent transvalvular pressure increasing from 0 up to 120 mm Hg was applied on the ventricular surface of the MV leaflets as a boundary condition characterizing the decoupled behavior of blood. The model was prepared for dynamic analysis in the time frame between end-diastole, at which the MV can be assumed as approximately unloaded, and peak systole, at which ventricular pressure reaches its maximum, while the MV remains closed. At peak systole, significant biomechanical parameters, such as tension forces in the chordae tendineae, reaction forces on the PMs, or stress distribution across the MV leaflets, reach their maximum values, thus
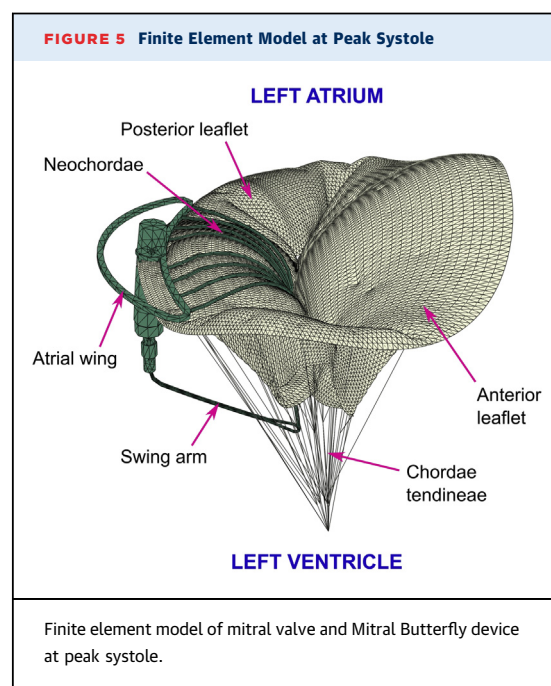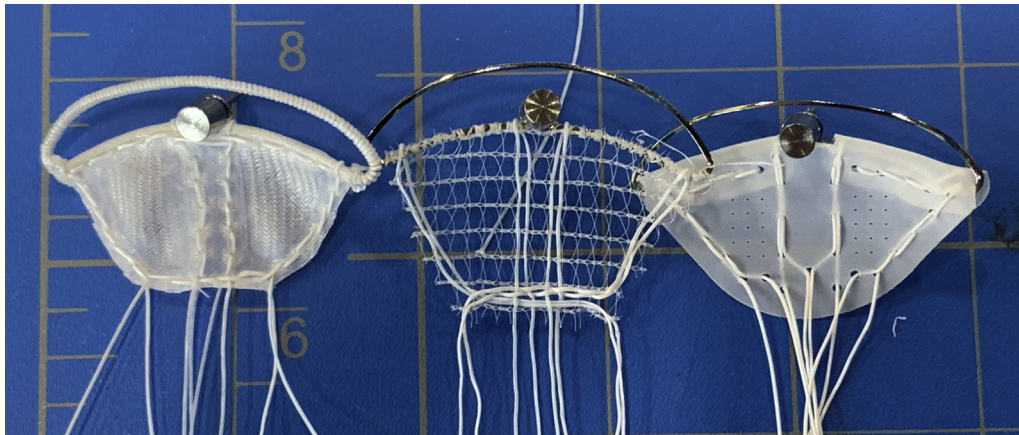

FIGURE 5   Finite Element Model at Peak Systole

Finite element model of mitral valve and Mitral Butterfly device at peak systole.

FIGURE 6 **Depiction of the 3 Test Article Designs**

The design/composition of the Polyethylene terephthalate meshes differed in the 3 implants (from left to right: USBio mesh [United States Biological Life Sciences, Salem, Massachusetts], Atex mesh [Atex Technologies Inc., Pinebluff, North Carolina], Sefar mesh [Sefar, Heiden, Switzerland]). Polyethylene terephthalate meshes had a thickness between 60 and 200 μm. The mesh structure was either based on warp knit or had pore sizes <50 μm.

simulating only the systolic function of the MV allows a reduction in computational time without sacrificing any results of interest.

In addition, a computational model of the Mitral Butterfly was created and prepared for the virtual implantation into the prolapsing MV model. The implant was composed of the following segments: 1) the body, consisting of needle, button, delivery tool locking collar, and upper and lower felt fittings, which keeps all the parts in place and positions the implant on the prolapsing MV leaflet; 2) the atrial wing, which stabilizes the implant in the LA and keeps the yarns spread out; 3) the swing arm, which collects the chordae into a central location and retains them to prevent a prolapse; and 4) 8 neochordae (instead of polymer mesh) that capture the prolapsing leaflet, thus restricting its bulging into the LA. All elements of the implant were assumed to be linear elastic and isotropic; their material parameters are shown in **Table 1**.

Two computational models were prepared for the simulation of the systolic function, representing the MV before (pre-repair) and after (post-repair) virtual implantation. The implant was positioned near the annulus of the post-repair model, and general contact with scale penalty method and friction coefficient of 0.05 was defined between its elements and the MV leaflets. For each model, the input file for the analysis in Abaqus/Explicit (Simulia, Dassault Systemes, Waltham, Massachusetts) was prepared and simulations of the systolic function were carried out.

The structure and morphology of the post-repair model at peak systole is shown in **Figure 5**. Note that after the virtual implantation of the Mitral Butterfly, prolapse of the P2 segment is eliminated.

CHRONIC ANIMAL STUDY. A chronic non-good laboratory practice (GLP) animal study was performed at American Preclinical Services (Minneapolis, Minnesota) to evaluate the performance and stability of the Mitral Butterfly chordal repair device in a porcine model for a duration of 90 days. The protocol

TABLE 2 **Computational Results at Peak Systole Before and After Virtual Implantation**

	Pre-Repair	Post-Repair
CoA, mm^2	209.0	325.2
CoL, mm	–	3.6
F_{PM}, N		
Anterolateral PM	6.24	5.37
Posteromedial PM	5.69	4.71
F_{SA}, N	–	1.30
F_{CT}, N	1.11	0.62
F_{NC}, N	–	0.42
S_1^L, MPa	1.55	0.48
S_1^{SA}, MPa	–	242.6

Dashes indicate data are not available.

CoA = coaptation area; CoL = coaptation length; F_{CT} = maximum tension force in the native chordae; F_{NC} = maximum tension force in the neochordae; F_{PM} = reaction force on the papillary muscle; F_{SA} = reaction force on the swing arm of the implant; S_1^L = peak value of the maximum principal stress acting on the leaflets; S_1^{SA} = peak value of the maximum principal stress acting on the swing arm of the implant.

FIGURE 7   Stress Patterns Across MV Leaflets

Stress patterns across the mitral valve (MV) leaflets with posterior leaflet displayed separately before **(A)** and after **(B)** virtual implantation of Mitral Butterfly device. Stress is acting on the neochordae **(C)** and the swing arm of the implant **(D)**.
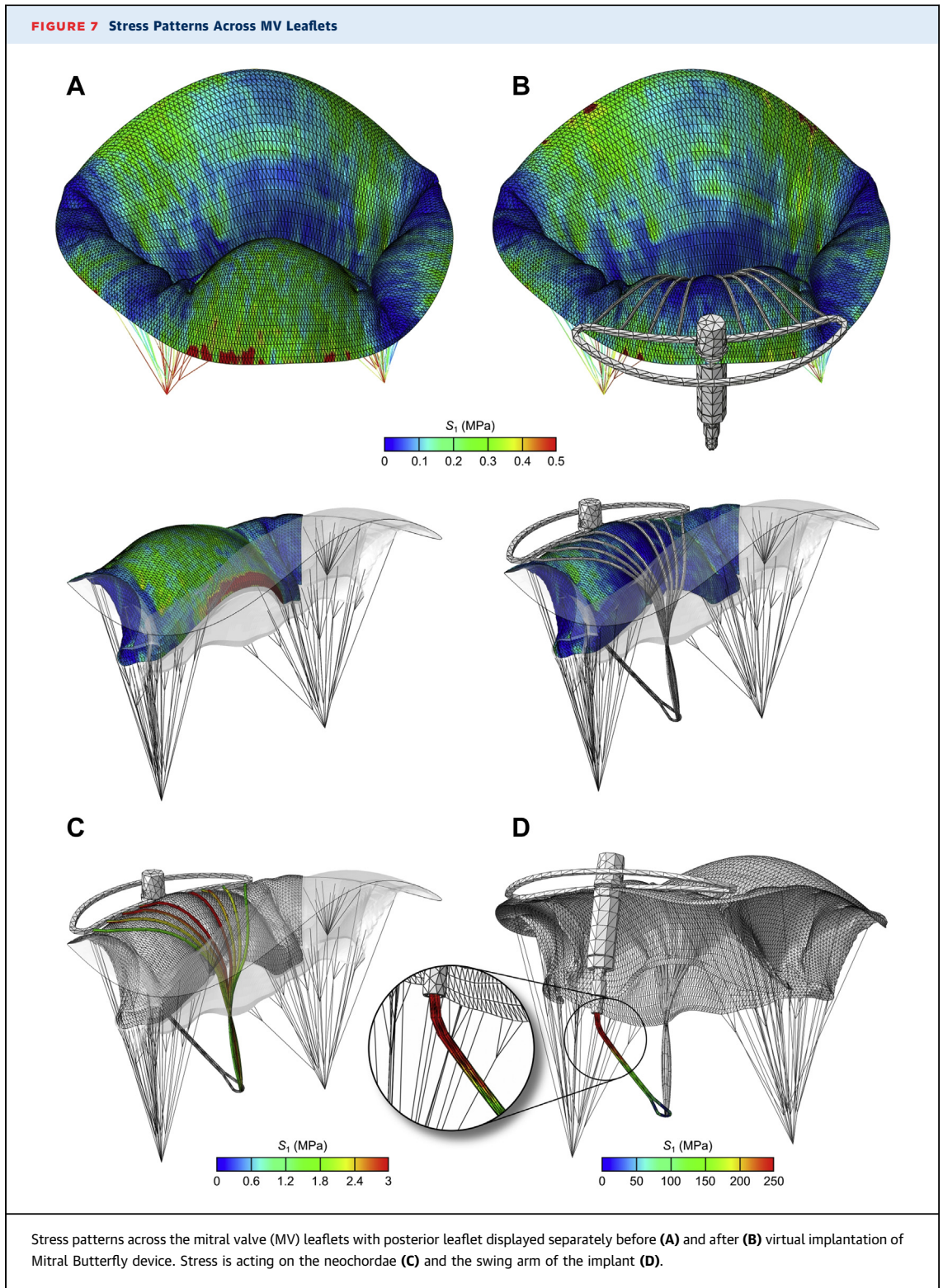
TABLE 3 Chronic Animal Study Results

	90-Day Follow-Up
Procedural success	100%
Mean bypass time	32.7 ± 10.3 min
Mean deployment time	1.3 ± 0.44 min
Device-related deaths	0

Seven Yorkshire cross swine, weighing 75 to 85 kg, were used.

was approved by the Institutional Animal Care and Use Committee prior to the study.

Study endpoints included interdevice comparison of 3 test article designs (Figure 6) and tissue response to the respective devices. The devices solely differed in design/composition of the polymer mesh. The 3 test article designs were made of PET meshes with a thickness between 60 and 200 μm. The mesh structure was either based on a warp knit or had pore sizes <50 μm. Each design was tested in 2 pigs.

Seven adult swine (Yorkshire cross, 75 to 85 kg range; Manthei Hog Farm LLC, Elk River, Minnesota) underwent left thoracotomy, and after preparation of the animals, cardiopulmonary bypass was initiated. Through a superior transatrial approach, the 24-F device delivery tool was introduced into the LA and passed through the MV. After reaching the LV, the delivery system was positioned to allow it to grab the target MV leaflet. Some loose suture loops were placed around chordae on either side of the P2 target location before the device was deployed on the intact posterior leaflet. Post-deployment, the sutures were removed, the delivery tool was retrieved, the heart closed, and the functionality of the implant confirmed using epicardial echocardiography and fluoroscopy. These procedures were performed in a standard operating room under anesthesia (isoflurane in 100% O_2, 0% to 5%, inhaled to effect; 2 to 8 mg/kg propofol). All animals were anticoagulated with 81 mg of aspirin and 150 mg of clopidogrel from the day before the implantation through to the terminal procedure. Heparin was administered as necessary during the implantation and terminal procedures. Imaging and hemodynamic data were collected to assess device performance approximately at 7, 30, 60, and 90 days post-procedure. To evaluate location and function of the implant and to assess its performance, transthoracic echocardiogram was used at 7- and 60-day follow-up, whereas intracardiac echo and fluoroscopy were used at the 30- and 90-day follow-up examinations. Four-dimensional gated cardiac computed tomography scans were performed for LA and LV volumes at termination. Following the

terminal procedure, the animals were euthanized and a focused necropsy on the heart/device implantation site was performed to observe ingrowth and tissue surrounding the implant.
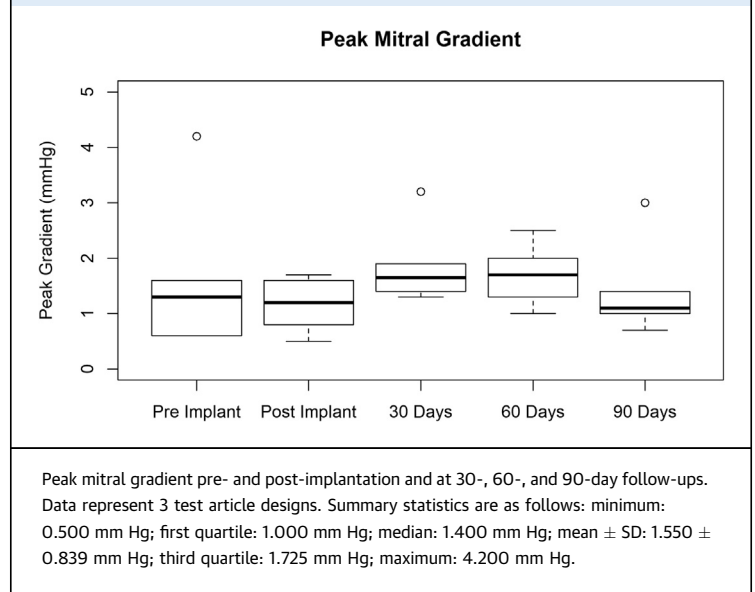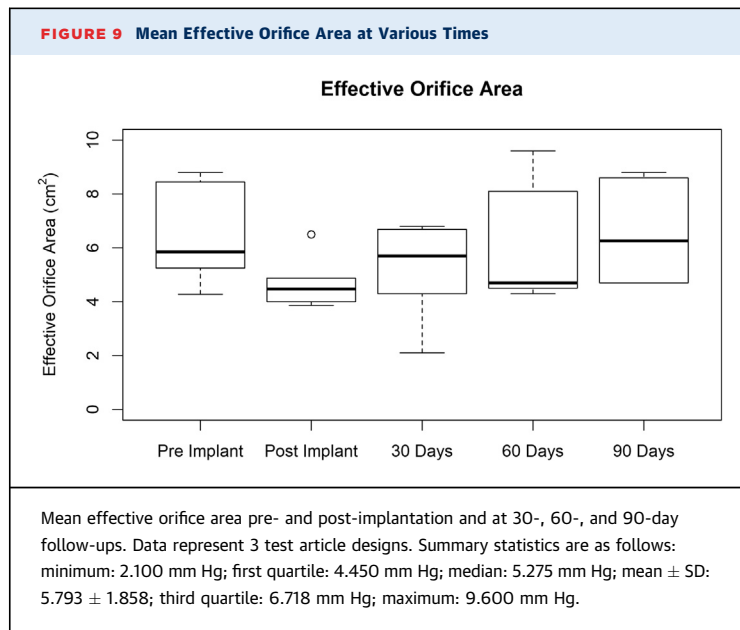
RESULTS

COMPUTATIONAL ANALYSIS. After each simulation, the following parameters were identified: 1) coaptation area and coaptation length of the leaflets; 2) reaction forces on the PMs and on the swing arm of the implant; 3) maximum tension forces in the native chordae and the neochordae; and 4) peak value of the maximum principal stress acting on the leaflets and on the swing arm. The values of the computed parameters (if present) are shown in Table 2.

Before the implantation of the Mitral Butterfly, a lack of contact between MV leaflets due to the prolapsing P2 segment was present. The virtual implantation recovered this contact by reducing the bulging of the posterior leaflet, increasing the coaptation area by 55.6%, and restoring the coaptation length of 3.6 mm.

The highest tension forces in the chordae tendineae before the virtual implantation appeared in the marginal chordae neighboring the prolapsing P2 segment with a peak value of 1.11 N. The virtual implantation of the Mitral Butterfly led to the elimination of the posterior leaflet bulging and partial relaxation of the native chordae. Therefore, the maximum chordal tension force in the post-repair model was reduced to 0.62 N. In addition, the tension forces in the

FIGURE 8 Peak Mitral Gradient at Various Times

Peak mitral gradient pre- and post-implantation and at 30-, 60-, and 90-day follow-ups. Data represent 3 test article designs. Summary statistics are as follows: minimum: 0.500 mm Hg; first quartile: 1.000 mm Hg; median: 1.400 mm Hg; mean ± SD: 1.550 ± 0.839 mm Hg; third quartile: 1.725 mm Hg; maximum: 4.200 mm Hg.

FIGURE 9   Mean Effective Orifice Area at Various Times

Mean effective orifice area pre- and post-implantation and at 30-, 60-, and 90-day follow-ups. Data represent 3 test article designs. Summary statistics are as follows: minimum: 2.100 mm Hg; first quartile: 4.450 mm Hg; median: 5.275 mm Hg; mean ± SD: 5.793 ± 1.858; third quartile: 6.718 mm Hg; maximum: 9.600 mm Hg.

neochordae of the implant were calculated according to the neochordal stress distribution (**Figure 7C**), showing the peak value to be 0.42 N.

In the pre-repair model, the reaction forces acting on the anterolateral and posteromedial PMs were 6.24 and 5.69 N, respectively. After the virtual implantation of the Mitral Butterfly, these forces were reduced to 5.37 and 4.71 N.

Also, in the pre-repair model (**Figure 7A**), a large stress concentration area neighboring the prolapsing P2 segment with a maximum stress value of 1.55 MPa, which exceeds the failure stress limit reported by Grande-Allen et al. (12), occurred. This excessive stress peak was reduced to a safe value of 0.48 MPa after the virtual implantation of the Mitral Butterfly (**Figure 7B**). Finally, stress patterns across the swing arm of the implant were investigated (**Figure 7D**), revealing the peak stress value of 242.6 MPa near the swing arm connection to the hypotube.

CHRONIC ANIMAL STUDY. Six swine were included in this chronic study. One animal died within 24 h of implantation procedure due to a non–device-related issue (swelling and erythema at the epiglottis and laryngeal folds). It was instantly replaced by a backup animal. Another animal was euthanized after 43 days of implantation due to increased stress; the remaining 5 swine were followed uneventfully for the entire duration of 3 months. Both premature terminations were non–device-related and the animals had competent valves with excellent device seating as demonstrated by echocardiography, contrast fluoroscopy, and gross examination following sacrifice.

All 7 implantation procedures were successful, and visual inspection confirmed excellent device positioning in all animals. Implant deployment took 80 ± 26 s on average (n = 7), the mean bypass time was <33 ± 10.3 min (**Table 3**).

All animals (except for the 1 that was pre-terminated after 43 days) had a weight gain of about 30% to 40% within 90 days. When performing repeated measures analysis of variance, no significant change in peak gradient (p = 0.713) could be observed pre- and post-implantation or within 90 days of follow-up (**Figure 8**) in any of the 6 pigs (3 test article designs). Ejection fraction remained constant at an average of approximately 60% in all animals. **Figure 9** depicts the effective orifice area pre- and post-implantation as well as at 30-, 60- and 90-day follow-ups. No trend could be observed among the 3 test article designs. The effective orifice area values for each animal at the various follow-up stages were compared using an analysis of variance, with no significant variation noted (p = 0.309).

Serial echocardiography demonstrated competent valves with sufficient coaptation at 30-, 60-, and 90-day follow-ups. Contrast angiographic and computed tomography findings were similar to echocardiograms. **Figure 10** shows that the Mitral Butterfly implant allows normal leaflet opening during diastole, while restricting excessive leaflet motion and enhancing coaptation during systole (Videos 4 to 7).

Imaging at 30-day follow-up showed little to no ingrowth of the device, and the PET cloth of the device moved completely independent from the native leaflet. At 60-day follow-up, trace MR was detected in 1 animal. Terminal echocardiographic imaging demonstrated stable device position, no MR in any of the animals with excellent valve closure and normal posterior leaflet motion. No signs of thrombosis or hemolysis were detected. Five animals remained clinically stable for the 3-month follow-up. The animals were sacrificed and intravital imaging was compared with postmortem gross anatomy. Post-mortem examination showed excellent device position with endothelialization at 3 months. Except for minor tissue abrasions on the anterior leaflet, no significant abnormalities were detected by gross examination. The amount of tissue ingrowth differed between the 3 mesh compositions (**Figure 11**); however, there is no indication that 1 mesh resulted in better ingrowth than others. In the 5 long-term survivors, the implanted device showed satisfactory healing (especially the encapsulation around the clasp was remarkable) with no inflammatory or toxicity response.

FIGURE 10 Depictions of Mitral Butterfly Implant
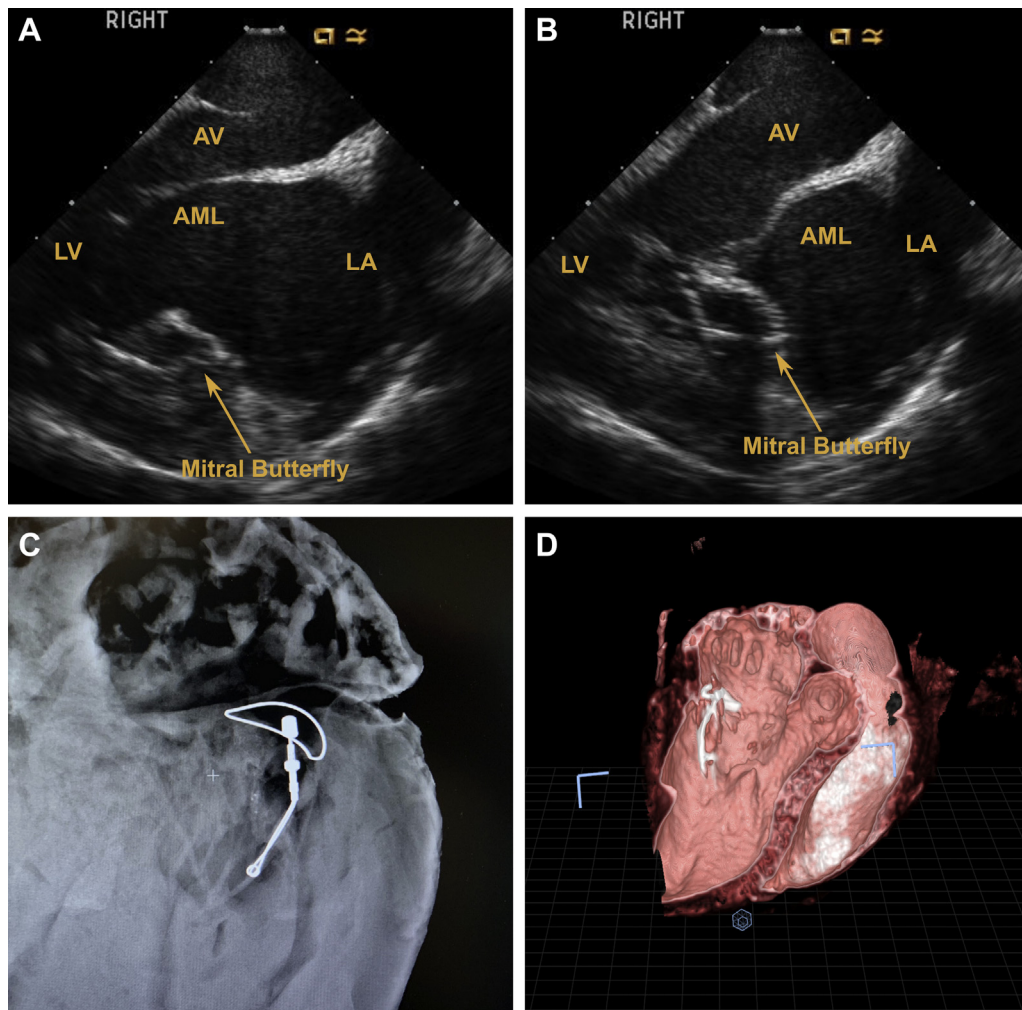
(A) A 30-day echocardiogram shows implant does not affect normal leaflet opening during diastole. (B) A 30-day echocardiogram shows the implant restricts excessive leaflet motion during systole and promotes sufficient coaptation. (C) Nitinol frame depicted via Faxitron (Faxitron Bioptics, Tucson, Arizona) during termination (90 days). (D) Computed tomography scan at 90 days shows position of Mitral Butterfly in the heart. Color echocardiograms and fluoroscopic appearance can be found in Videos 4, 5, 6, and 7. AML = anterior mitral leaflet; AV = atrioventricular; LA = left atrium; LV = left ventricle.

DISCUSSION

The artificial PM concept, embodied by the Mitral Butterfly device, has been demonstrated as a valid alternative to current chordal repair options. Pre-clinical studies evaluated the implantation process and showed excellent device acceptance and long-term stability. Additionally, the results obtained during computational analysis showed increased coaptation and reduced chordal tension. The parameters computed during the simulations of the MV systolic function were compared with those published in the previous computational works investigating different neochordal implantation techniques, in particular, the loop technique and transapical MV repair.

The calculated tension forces in the chordae tendineae (1.11 N reduced to 0.62 N) were in complete agreement with the forces reported in the previous work investigating the transapical MV repair (13), where the maximum chordal tension force of 1.10 N was reduced to 0.61 N after the elimination of the prolapse. Regarding the tension forces in the neo-chordae of the implant, the computed peak value of

FIGURE 11   Necropsy Images of the Mitral Butterfly at 90 Days
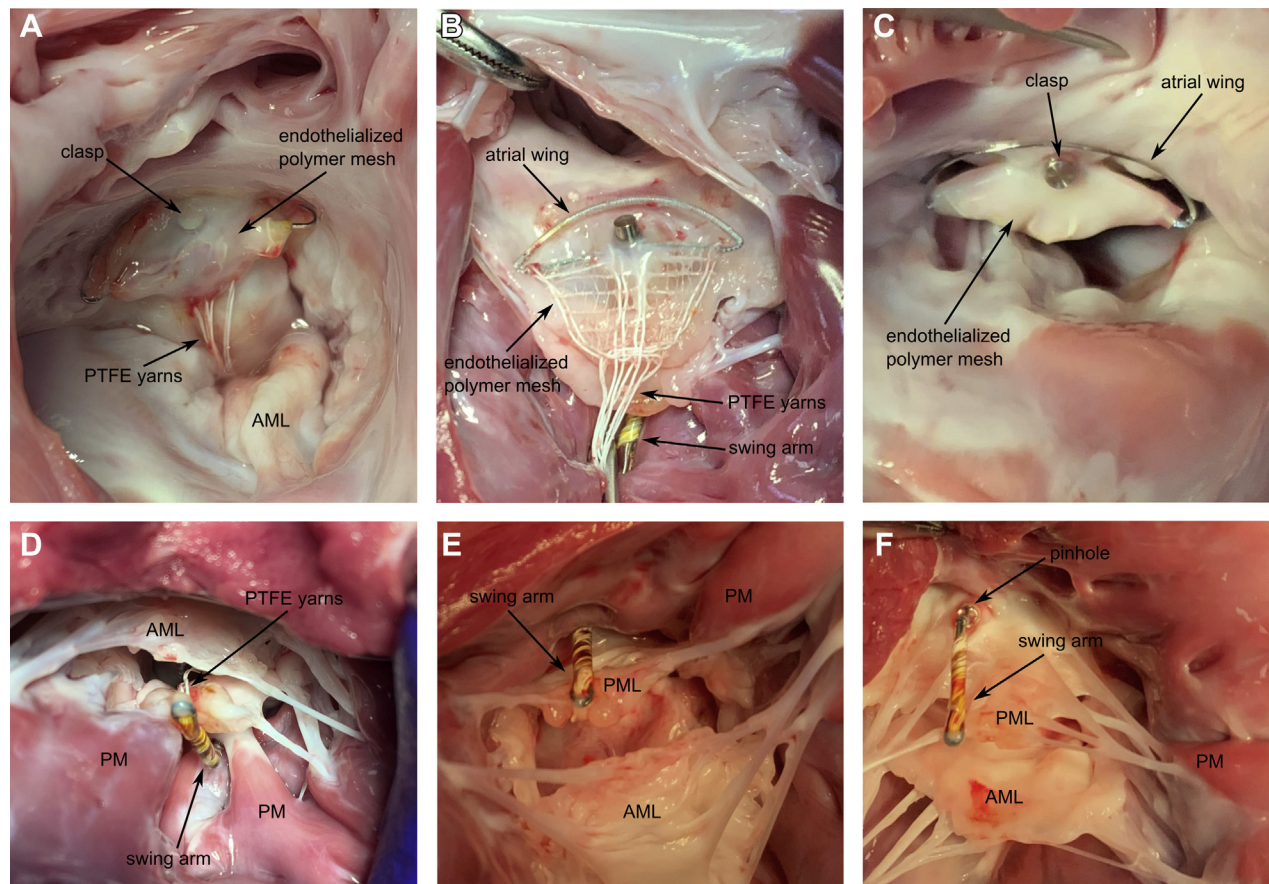
(A to C) Atrial views of the ingrowths of the 3 different mesh designs (USBio, Atex, Sefar, respectively) are shown. (D to F) Ventricular views of the swing arms are shown. Note the complete integration of the clasp surrounding the penetration site. AML = anterior mitral leaflet; PM = papillary muscle; PML = posterior mitral leaflet; PTFE = polytetrafluoroethylene.

0.42 N is significantly lower than the values reported in the studies quantitatively investigating different neochordal implantation techniques (12-14). Because, in this case, the neochordae are not implanted into the leaflet, the direction of the acting forces is completely different, thus the value of the maximum neochordal tension force is hardly comparable with those found in other published reports. Nevertheless, decent distribution of tension forces was observed with the highest values in the neochordae attached to the middle section of the Mitral Butterfly and the lowest in the ones attached to the flanks. Because such distribution of tension forces ensures the elimination of MV prolapse and proper seal of the valve, it can be assumed that the lower maximum force value was obtained due to the force distribution on the higher number of the neochordae (n = 8) used,

compared with the implantation of 3 to 4 neochordae described in the published data (12-14).

Regarding the reaction forces on the PMs, the calculated values and their reduction are very similar to those reported by other investigators (14,15). This reduction of reaction forces can be explained by the partial transfer of tension forces acting in the native chordae to the implant, creating reaction force on the swing arm equal to 1.30 N.

Stress analysis showed the computed stress patterns across the prolapsing MV leaflets to be similar to those found in other publications (16,17). In terms of stress distribution in the swing arm of the Mitral Butterfly, the peak value of 242.6 MPa can seem very high, in particular, if compared with stress distribution across the MV leaflets. However, the cross-sectional area of the arm-forming nitinol wire, which is only

0.114 mm², needs to be taken into the account to better understand the origin of such stress. In addition, the computed stress peak is lower than the yield strength of nitinol, which is up to 690 MPa. Therefore, such stress is not critical to the structure, because the swing arm is operating only in the elastic zone of the stress-strain curve, thus, plastic deformation of the structure is very unlikely.

The stability of the swing arm has also been successfully demonstrated in the chronic 90-day animal study, proving the feasibility of the artificial PM concept in a long-term in vivo model. Within 90 days, corresponding to approximately 10 million cycles, no fatigue or erosion issues were detected. Primary endpoints of this study were moribundity, interdevice comparisons, and tissue response to the device. In all 6 animals, the implanted device showed stable device position and satisfactory healing with all of the mesh compositions. The open mesh composition is preferred based on visual inspection. However, a 5-month study in an ovine model will be performed to further evaluate the mesh design. Although there were no signs of thrombosis, the potential for embolism was not assessed in this study. The necropsies in this study were targeted to only the heart tissue; neither brain nor kidneys were assessed for emboli.

Although deployment time in sequential mono-chordal mitral repair cannot be found in the scientific publications, the 1-step attachment of the Mitral Butterfly device within 80 s seems difficult to outperform. Whereas the devices were deployed on intact MV leaflets during this study, the Mitral Butterfly implant has already been successfully tested in a pulsatile heart model with iatrogenic chordal rupture prior to this study (see **Figure 2**). The efficacy of the device in myxomatous tissue has not been evaluated during this chronic study and whether the device works as well in tissue with a different elastic integrity remains to be tested.

STUDY LIMITATIONS. It should be noted that the study was limited to deployment in animals exhibiting no leaflet flail. Although it would have been possible to induce acute prolapse, it would not have

been possible to achieve the characteristic leaflet elongation and thickening observed in chronic prolapse cases without subjecting the animals to prolonged discomfort. Therefor the decision was made to proceed with healthy valve anatomy and evaluate the implant delivery and function independent of MR.

CONCLUSIONS

The features of the Mitral Butterfly device allow transcatheter MV repair, avoiding chordal fixation on myocardial structures and making the success of primary repair independent from future ventricular dynamics. The transseptal version may allow the recruitment of more patients, even those with limited symptoms of heart failure.

AUTHOR RELATIONSHIP WITH INDUSTRY

ADDRESS FOR CORRESPONDENCE: Dr. Werner Mohl, Medical University of Vienna, AVVie GmbH, Lazarettgasse 12/1, 1090 Vienna, Austria. E-mail: wmohl@angelvalve.com.

PERSPECTIVES

COMPETENCY IN MEDICAL KNOWLEDGE: Transcatheter MV repair strategies, compared with the surgical standard, offer a less invasive procedural approach for the treatment of patients affected by MR. In this case, because of the deployment strategy, the Mitral Butterfly also, boasts a competitive procedural time and demonstrates a high potential for clinical application.

TRANSLATIONAL OUTLOOK: The Mitral Butterfly offers a completely different approach to correct prolapsing segments. Unlike monochordal replacement the device allows a 1-step implantation and is designed to reduce the learning curve for interventionists. Further studies are needed to confirm the efficacy of this MV repair implant in patients with MR.

REFERENCES

1. Delling FN, Vasan RS. Epidemiology and pathophysiology of mitral valve prolapse: new insights into disease progression, genetics, and molecular basis. Circulation 2014;129:2158–70.

2. Chiam PT, Ruiz CE. Percutaneous transcatheter mitral valve repair: a classification of the technology. J Am Coll Cardiol Intv 2011;4:1–13.

3. Gillinov M, Mick S, Suri RM. The specialty of mitral valve repair. J Am Coll Cardiol 2017;69: 2407–9.

4. Colli A, Fiocco A, Pradegan N, Nadali M, Besola L, Bizzotto E, Gerosa G. Transcatheter chordal repair for degenerative mitral regurgitation. Cardiac Interv Today 2018;12:45–9.

5. Sturla F, Votta E, Onorati F, et al. Biomechanical drawbacks of different techniques of mitral neochordal implantation: when an apparently optimal repair can fail. J Thorac Cardiovasc Surg 2015;150: 1303–12.e4.

6. Grinberg D, Adamou Nouhou K, Pozzi M, Obadia JF. Artificial mitral chordae: when length

matters. J Thorac Cardiovasc Surg 2019;157: e23–5.

7. Koprivanac M, Kelava M, Alansari S, et al. Degenerative mitral valve disease-contemporary surgical approaches and repair techniques. Ann Cardiothorac Surg 2017;6:38–46.

8. Gaidulis G, Votta E, Selmi M, Aidietiene S, Aidietis A, Kacianauskas R. Numerical simulation of transapical off-pump mitral valve repair with neochordae implantation. Technol Health Care 2018;26:635–45.

9. Stevanella M, Maffessanti F, Conti CA, et al. Mitral valve patient-specific finite element modeling from cardiac MRI: application to an annuloplasty procedure. Cardiovasc Eng Technol 2011;2:66–76.

10. Kunzelman KS, Einstein DR, Cochran RP. Fluid-structure interaction models of the mitral valve: function in normal and pathological states. Philos Trans R Soc Lond B Biol Sci 2007;362:1393–406.

11. Lee CH, Amini R, Gorman RC, Gorman JH III, Sacks MS. An inverse modeling approach for stress

estimation in mitral valve anterior leaflet valvuloplasty for in-vivo valvular biomaterial assessment. J Biomech 2014;47:2055–63.

12. Grande-Allen KJ, Barber JE, Klatka KM, Houghtaling PL, Vesely I, Moravec CS, McCarthy PM. Mitral valve stiffening in end-stage heart failure: evidence of an organic contribution to functional mitral regurgitation. J Thorac Cardiovasc Surg 2005;130:783–90.

13. Gaidulis G, Selmi M, Zakarkaitė D, Aidietis A, Kačianauskas R. Modelling and simulation of mitral valve for transapical repair applications. Nonlinear Analysis Model Control 2019;24: 485–502.

14. Caballero A, Mao W, McKay R, Sun W. Transapical mitral valve repair with neochordae implantation: FSI analysis of neochordae number and complexity of leaflet prolapse. Int J Numer Method Biomed Eng 2020;36:e3297.

15. Sturla F, Onorati F, Votta E, et al. Repair of mitral valve prolapse through ePTFE neochordae: a finite element approach from CMR. In: Lenarz T,

Wriggers P, editors. Biomedical Technology. Heidelberg, Germany: Springer Verlag, 2015:117–28.

16. Rim Y, Laing ST, McPherson DD, Kim H. Mitral valve repair using ePTFE sutures for ruptured mitral chordae tendineae: a computational simulation study. Ann Biomed Eng 2014; 42:139–48.

17. Sturla F, Onorati F, Votta E, et al. Is it possible to assess the best mitral valve repair in the individual patient? Preliminary results of a finite element study from magnetic resonance imaging data. J Thorac Cardiovasc Surg 2014; 148:1025–34.

KEY WORDS chordal repair, computational analysis, finite element analysis, transcatheter mitral valve repair

APPENDIX For supplemental methods and videos, please see the online version of this paper.